TECHNICAL ARTICLE—PEER-REVIEWED

Experimental Verification and Nonlinear Dynamic Response Analysis of a Rolling Element Bearing with Localized Defects

Abdelgawad H. A. Mattar · Hussien Sayed · Younes K. Younes · Heba H. El-Mongy

Abstract In this paper, the dynamic behavior of rolling element bearings with localized faults on the inner and outer rings is investigated. A nonlinear mathematical model is developed with five degrees of freedom considering rotor unbalance. In this bearing model, the nonlinearity is caused by the Hertzian contact forces and the radial internal clearance. The fourth-order Runge–Kutta technique is used to solve the coupled nonlinear equations of motion numerically. Nonlinear vibration response of the rotor and bearing housing can be obtained in both time and frequency domains. An experimental verification of the numerical model is presented where experimental measurements for defective ball bearings are compared with the numerical results. Envelope spectra of the numerical results show similar behavior to that of the measured experimental signals. A parametric analysis is conducted to investigate the effect of system parameters on the nonlinear dynamic response using time waveforms, orbit plots, frequency spectra and bifurcation diagrams. The presented results demonstrate that the dynamic response shows periodic, quasi-periodic and chaotic motions because of varying rotational speeds and defect width. The proposed model contributes toward improved design and better health monitoring of bearings in practice.

List of symbols

C_h :	Equivalent viscous damping of housing, N-s /m
C_s :	Equivalent viscous damping of shaft, N-s /m
C_r :	Equivalent viscous damping of unit resonator, N-s /m
C :	Clearance in radial direction, m
D	Bearing pitch diameter, m
d	Diameter of ball, m
e :	Radius of mass unbalance, m
F_x :	The bearing's nonlinear contact force in the horizontal direction, N
F_y :	The bearing's nonlinear contact force in vertical direction, N
F_{un} :	The unbalance force, N
K	Contact stiffness of the bearing, $N/m^{3/2}$
K_h :	Equivalent stiffness of housing, N/m
K_s :	Equivalent stiffness damping of shaft, N/m
K_r :	Equivalent stiffness damping of unit resonator, N/m
M_h :	The total mass of the housing, including mass of the outer ring, kg
M_s :	The total mass of the shaft, including mass of the inner ring, kg
M_r :	Total mass of unit resonator, kg
m_{un} :	Unbalance mass, kg
N_b :	Number of rolling elements
Q	Contact force at any ball position
t	Time, s
X, Y	Deflection along the axes, m
ω_c :	The angular velocity of the cage, rad/s

A. H. A. Mattar · H. Sayed · Y. K. Younes · H. H. El-Mongy (✉)
Department of Mechanical Design, Faculty of Engineering-Mataria, Helwan University, Cairo, Egypt
e-mail: heba_almongy@m-eng.helwan.edu.eg

H. H. El-Mongy
Centre for Applied Dynamics Research, School of Engineering, University of Aberdeen, Aberdeen, UK

1754

J Fail. Anal. and Preven. (2022) 22:1753–1770

ω_s :   Shaft rotational speed, rad/s

α Angle of contact relative to the X-axis, rad

Δ :   Deflection of the ball center in the defective zone, m

δ Contact deflection in the radial direction, m

θ Whirling angle of the shaft around its axis, rad

φ :   Ball angular location, rad

φ_o :   Angle between two balls, rad

ψ :   Angular displacement of shaft, rad

Introduction

Rolling element bearings are crucial machine components that are widely employed in rotating machinery. Bearing faults directly affect machine performance and may cause production losses and decreased machine service life, or even may lead to catastrophic failures. Singh and Al Kazzaz [1] indicated that bearing fault is the most common mechanical fault in induction motors and can be the root cause of other mechanical faults such as eccentricity and rotor–stator rubbing. Hence, early detection and diagnosis of defects in rolling bearings is essential in order to avoid unexpected failures and to ensure safe operation of machinery.

In the past decades, much attention has been given to developing techniques for early detection and diagnosis of bearing faults which have been well documented in several reviews [2–6]. Bearing damage may arise from manufacturing imperfections or assembly errors but sometimes it may occur due to harsh operating conditions causing increased stresses on the bearing. Defects in rolling element bearings can be categorized into local defects such as pits, spalls and cracks in the rings or rolling elements, and distributed defects such as surface roughness, waviness and misaligned rings [7–9]. This gives rise to significant changes in the bearing vibration response. There are two research pathways to investigate bearing response to defects. The first is conducting experimental studies whether seeded laboratory tests or monitoring real bearings in industrial equipment. In most cases, signal processing techniques are applied to extract bearing defect features from the measured vibration signals [10–15]. The second approach is to build precise mathematical models that accurately replicate the actual rotor-bearing systems and investigate the influence of defects on the response. The results of such models play a crucial role in developing better understanding of the phenomena associated with bearing failure.

Extensive research studies were conducted to develop mathematical models that investigate the vibration response of rolling element bearings with localized defects.

When a local defect starts to develop within a ball bearing, a sudden change in the contact force between the ring and the ball will occur [16]. McFadden and Smith [17] introduced a simple bearing model that represented the impact between a single point defect and bearing surface as an impulse. Hence, the resulting vibration signal can be represented as a series of periodic impulses that may excite resonances in the bearing. The period of these impulses depends on the location of the defect, whether it is on the outer ring, inner ring or on the rolling element. In [18], McFadden and Smith extended their model to study multiple point defects. Tandon and Choudhury [19] presented an analytical model bearing vibration response due to local defects on the inner ring, outer ring or a rolling element considering different pulse forms. Patil et al. [20] modeled the defect as a half sinusoid and predicted the vibration characteristics in time and frequency domains. The effect of defect size, load and speed was investigated, and the theoretical results were validated experimentally showing good agreement in predicting the frequency components. Changqing and Qingyu [21] studied the effect of surface waviness and clearance between the balls and rings on the dynamic stability and vibration response of a rotor bearing system. Recently, Zhang et al. [22] studied numerically and experimentally the dynamics of compound bearing fault in rolling element and outer ring.

Most of the studies modeled the nonlinear contact forces using the Hertzian contact theory for point contact such as [23–26]. Liqin et al. [23] conducted a bifurcation analysis to study the effects of various parameters such as rotational speed, radial force, damping, clearance, unbalance and waviness on the nonlinear dynamic behavior of a roller bearing system. Arslan and Akturk [24] investigated the vibrations of an angular contact ball bearing with and without defects in both time and frequency domains. Kankar et al. [25] focused on the analysis of bearing responses to localized faults for accurate performance prediction. Rafsanjani et al. [26] studied the stability of a rolling bearing system with localized surface defects.

Ideally, the bearing response will show periodic impulses with the evolution of bearing characteristic frequencies (BCFs) that indicate bearing fault [16]. However, unpredictable dynamic behavior of rotor-bearing systems has been recorded in literature and documented in several experimental case studies due to the nonlinear phenomena associated with these systems [3]. The influence of bearing nonlinearities such as Hertzian contact force, bearing clearance and varying compliance on the bearing nonlinear dynamic response has been investigated. Various nonlinear responses were observed such as quasi-periodic and chaotic motions. Tiwari et al. [27] studied the effect of radial internal clearance on the bearing response and showed that the increase in bearing clearance will widen the

unstable and chaotic regions in the bearing response. Harsha [28] studied analytically the nonlinear response of an unbalanced rotor supported on roller bearings and observed the routes to chaos to be intermittency regimes and period doubling. Ghafari et al. [29] showed experimentally the occurrence of chaos in the bearing response and presented a numerical analysis of the chaotic vibrations due to different localized faults in the bearing. Gupta et al. [30] investigated the effect of rotating unbalance and bearing clearance on the stability, chaos and quasi-periodic response of a rotor-bearing system.

Many attempts have been made by researchers to improve bearing models to better describe contact at the defect interface and to investigate the effect of different system parameters on the response of defective bearings. Tadina and Boltežar [31] presented an improved model of the defect geometry in which the local defects on the rings are represented by an impressed ellipsoid and as a flattened sphere for the balls. The improved bearing model is then coupled with the FE model of the housing to get the vibration response during run up. Cong et al. [32] presented a bearing model based on the analysis of defect load on the surface of the bearing and investigated its effect on the envelope spectrum. Pandya et al. [33] studied the effect of combined localized defects on the vibration response of high speed ball bearings. Cui et al. [34] presented an improved fault model by considering the variation of deformation according to the size ratio of the defect and the ball and the ratio of defect length to width. Cui et al. [35] developed a nonlinear vibration model that helps in identifying the impact points from the vibration signal which contributes to fault severity assessment. Mishra et al. [36] evaluated three different bearing models by extracting frequency domain features from vibration signal under different bearing faults and comparing with experiments. Kappaganthu and Nataraj [37] presented a nonlinear bearing model that focuses on the effect of clearance taking into account the offset between the centerlines of the inner and outer rings. Rehab et al. [38] studied the effect of internal bearing clearances that occur during bearing service life due to wear. Kong et al. [16] proposed a vibration bearing model based on the Hertzian contact stress distribution that focuses on the analysis of the contact between ball and defect. It was shown that the sinking depth of the balls and the geometry at the contact, not only depends on defect width and ball radius, but also on the bearing load. Wang et al. [39] presented an improved nonlinear model to accurately obtain deformations at contact considering preloading, load distribution analysis, Hertzian contact, rotor eccentricity, elastohydrodynamic lubrication and surface waviness. Kong et al. [40] studied the influence of damping on the nonlinear response of defective bearings by considering different levels of viscosity of grease. Wang
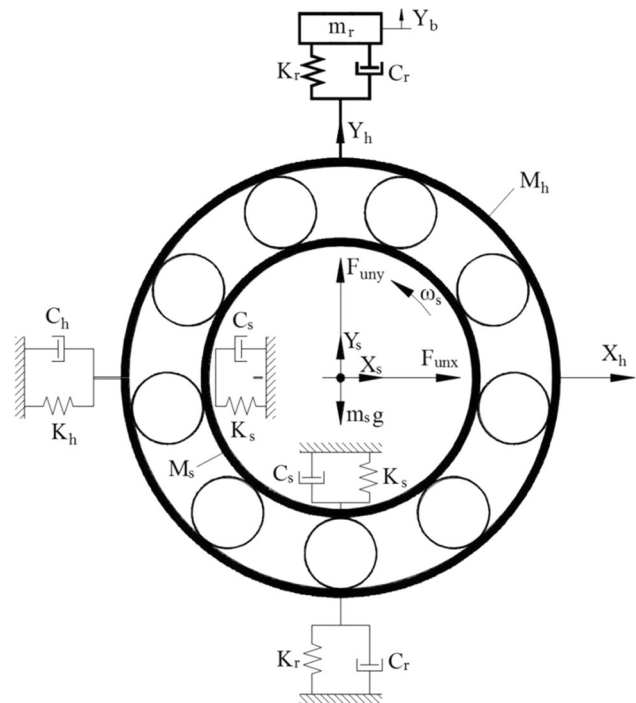
Fig. 1 Lumped parameter of a mathematical model of the rolling bearing-shaft-housing system

et al. [41] developed a bearing model with improved dynamic load distribution to monitor bearing clearance. Recently, Liang et al. [42] introduced a finite element model to study the effect of rolling bearing parameters on the vibration response of an offset rotor without faults.

In this paper, a nonlinear dynamic model of a rolling element bearing with localized surface defects on the inner and outer rings is developed. The contact forces are modeled using the nonlinear Hertzian contact theory. The coupled nonlinear equations are solved using Runge–Kutta algorithm. The model is verified experimentally for both time and frequency domains. Furthermore, a detailed parametric study is conducted to explore the effect of system parameters on the nonlinear response, namely rotational speed and defect width. The outline of the rest of the paper is organized as follows: Sect. "Modeling Rolling Bearings with Local Defects" presents the nonlinear model of the bearing system. The experimental setup is described in Sect. "Experimental Setup". The experimental verification is given in Sect. "Experimental Verification" where the numerical results are compared with experimentally acquired signals from defective bearings. The effect of bearing system parameters on the vibration response is demonstrated in detail in Sect. "Parametric Study". Finally, the main conclusions are summarized in Sect. "Conclusions".

Modeling Rolling Bearings with Local Defects

Rolling Element Bearing Model

In this section, a mathematical model of the rolling bearing-shaft-housing system is introduced. Figure 1 shows the lumped parameter model of the rolling bearing system. A five-degrees-of-freedom (DOF) model is assumed where the fifth degree of freedom represents a unit resonator with small mass and high stiffness and damping to enable simulating high-frequency resonant response in the vertical direction [35, 38]. The shaft-housing system under consideration is represented by M_s which represents the shaft's mass including the mass of the inner ring, M_h that denotes the mass of the housing including mass of the outer ring, and M_r which represents the mass of the unit resonator. The balls' masses are assumed to be negligible because their mass is considered small in comparison with other bearing components. The balls are assumed to be positioned equidistantly around the shaft center without touching each other and no slip occurs while rolling over the ring surface. All damping is linearly viscous damping where lubrication damping is not considered in this model.

The governing equations of motion describing displacements of the mass of the shaft, housing and unit resonator can be derived based on the abovementioned assumptions and considerations. As illustrated in Fig. 1, the governing equations of motion in X and Y axes are written as follows [35, 38]:

- For the shaft:

$$M_s\ddot{X}_s + C_s\dot{X}_S + K_sX_s + F_x = F_{un}\cos(\psi) \quad (Eq\ 1)$$

$$M_s\ddot{Y}_s + C_s\dot{Y}_S + K_sY_s + F_y = F_{un}\sin(\psi) - M_sg \quad (Eq\ 2)$$

- For the housing:

$$M_h\ddot{X}_h + C_h\dot{X}_h + K_hX_h - F_x = 0 \quad (Eq\ 3)$$

$$M_h\ddot{Y}_h + (C_h + C_r)\dot{Y}_h + (K_h + K_r)Y_h - C_r\dot{Y}_b + K_rY_b - F_y = 0 \quad (Eq\ 4)$$

- For the unit resonator:

$$M_r\ddot{Y}_b + C_r(\dot{Y}_b - \dot{Y}_h) + K_r(Y_b - Y_h) = 0 \quad (Eq\ 5)$$

where M_s, C_s, K_s, M_h, C_h, K_h, M_r, C_r and K_r represent the mass, damping and stiffness of inner ring, outer ring and unit resonator, respectively. The displacements X_s, Y_s, X_h, Y_h and Y_b describe the displacements of inner ring, outer ring in horizontal and vertical directions, and vertical displacement of the unit resonator, respectively. The unbalance force F_{un} that results due to unbalance mass [9, 40] can be defined as:

$$F_{un} = m_{un}e\omega_s^2 \quad (Eq\ 6)$$

where m_{un} is the unbalance mass, e is the eccentricity and ω_s is the rotational speed of the shaft, while ψ is the angular displacement of shaft and equals ω_st for constant speed rotors. The nonlinear contact forces of the bearing in
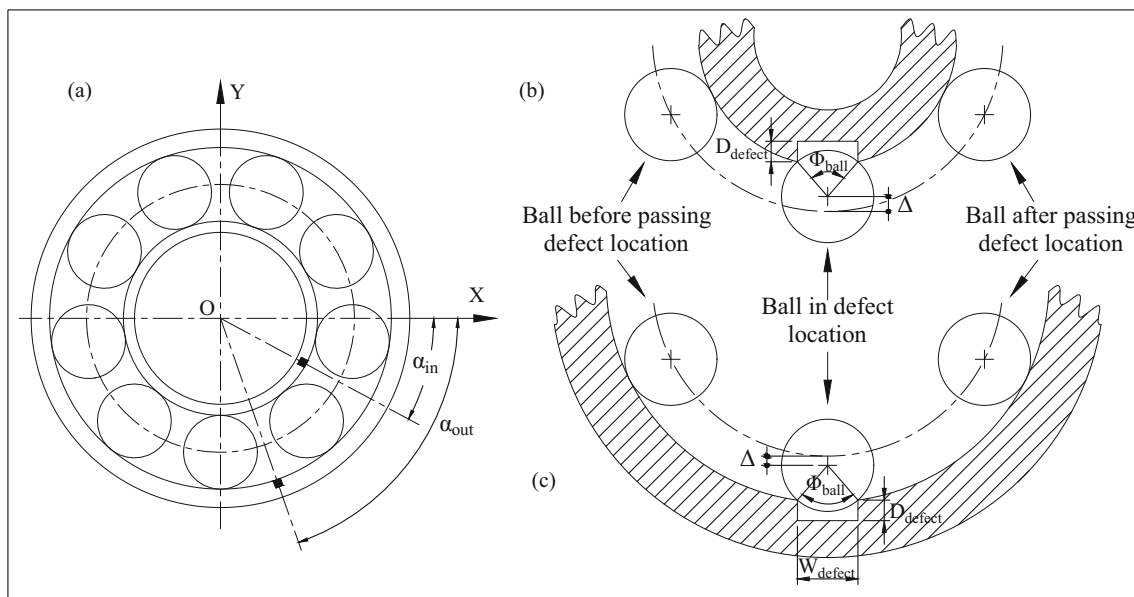
Fig. 2 Description of the faults and deflections: (a) graphical location of the faults, (b) additional deflection of the ball related to defect on inner ring and (c) additional deflection of the ball related to defect on outer ring [43]

the horizontal and vertical directions are represented by F_x and F_y, respectively.

Nonlinear Contact Forces

Nonlinear Hertzian contact deformations are considered for interactions between balls and rings. The nonlinear contact forces are determined by adding the restoring forces produced from each individual rolling element in the X and Y directions, as shown in Eqs 7 and 8 [38]:

$$F_x = \sum_{i=1}^{N_b} k[\delta_i]^{\frac{3}{2}} cos\varphi_i \qquad \text{(Eq 7)}$$

$$F_y = \sum_{i=1}^{N_b} k[\delta_i]^{\frac{3}{2}} sin\varphi_i \qquad \text{(Eq 8)}$$

where N_b is the number of rolling elements, k is the Hertzian contact stiffness, δ is the contact deformation, and φ_i is the ball angular location.

Equation 9 can be used to describe the total contact deformation δ for the ith ball which is given as a function of the shaft movement relative to the housing in the X and Y axes, the radial clearance C and the ball angular position φ_i. The term Δ represents additional deflection that results from the short-duration pulse which occurs when the rolling element gets in contact with the defect.

Fig. 3 PT500 test rig used for experimental work

Table 2 The rolling element bearing's geometrical and physical features

Parameter	Detail
Rolling elements number,N_b	9
Rolling element diameter, d	0.0066 m
Pitch diameter, D	0.031 m
Angle of contact, α	0
Clearance in radial direction, C	0.000005 m
Contact stiffness, k	9.62127 N$\times10^9$/m$^{3/2}$
Stiffness of outer ring K_h	18 N$\times10^6$/m
Stiffness of the shaft K_s	2.79262 N$\times10^5$/m
Stiffness of unit resonator K_r	9 N$\times10^9$/m
Damping of the outer ring C_h	1000 N-s/m
Damping of the shaft C_s	317.4 -s/m
Damping of unit resonator C_r	9000 N-s/m
Mass of unit resonator,M_r	0.057 kg
Mass of the inner ring,M_s	2.836 kg
Mass of the outer ring,M_h	0.806 kg
Width of defect, W	0.0005 m

Table 1 Dimensions of test rig components

Component	Parameter	Detail
Shaft	Shaft length	0.5 m
	Shaft diameter	0.02 m
	Bearing span	0.35 m
	Modulus of elasticity of shaft material	2 N$\times10^{11}$/m^2
	Density	7850 kg/m^3
Disk	Disk outer diameter	0.15 m
	Disk inner diameter	0.02 m
	Disk thickness	0.01122 m
	Mass of disk	1.52 kg
	Mass unbalance, m_{un}	0.009158 kg
	Radius of mass unbalance	0.06 m
Bearing	Type	Single deep groove ball bearing Type SKF 6004-2ZR

$$\delta_i = (X_s - X_h)\cos\varphi_i + (Y_s - Y_h)\sin\varphi_i - C - \Delta \quad \text{(Eq 9)}$$

The springs must only function in compression conditions because Hertzian forces occur only when there is a loaded contact. In other words, when the instantaneous spring length is less than the unstressed length, the appropriate spring force is produced with a positive value of the deflection δ. Instead, when the ball and the ring separate, the restoring force is reset to zero. As a result, Eq 10 can be used to describe the contact force Q at any ball position [35]:

$$Q = \begin{cases} k[\delta_i]^{3/2} & \delta > 0 \\ 0 & \delta \leq 0 \end{cases} \quad \text{(Eq 10)}$$

The angular location φ_i of the rolling elements can be described as a function in the cage speed ω_c, initial angular position of the bearing cage φ_0 and time t. Equation 11 is used to define the ball angular location [43]:

$$\varphi_i = \frac{2\pi(i-1)}{N_b} + \omega_c t + \varphi_0 \quad \text{(Eq 11)}$$

The angular velocity of the shaft ω_s is used to describe the angular velocity of the cage ω_c as follows [43]:
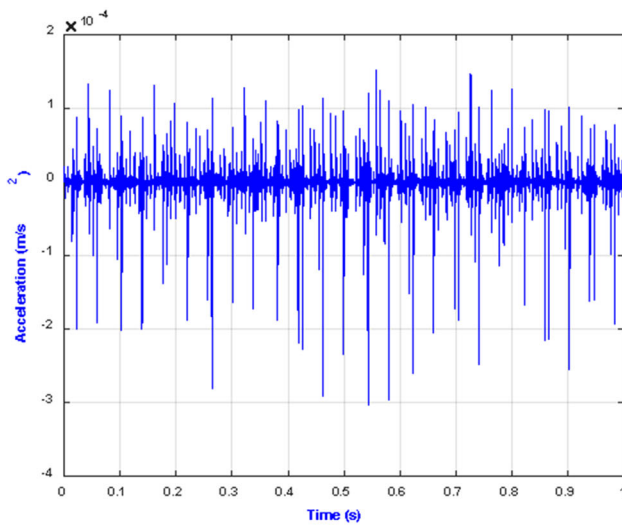
(a)
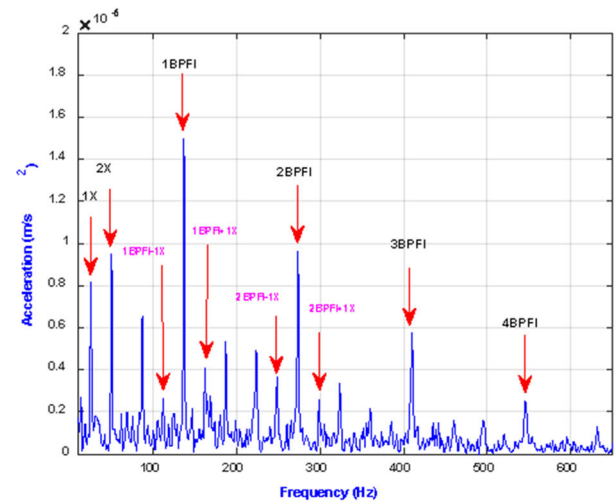
(b)
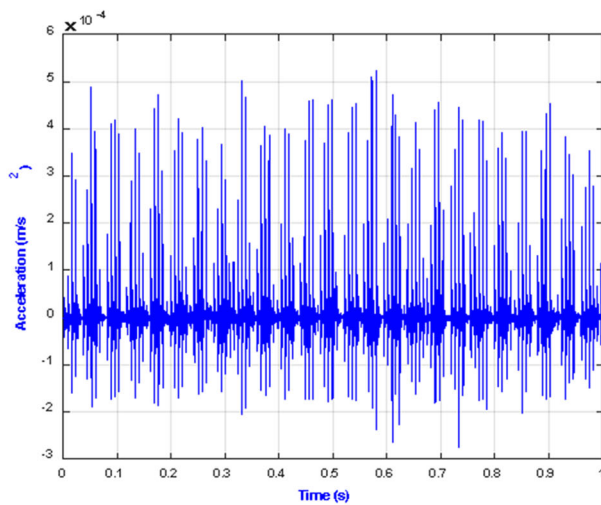
(c)
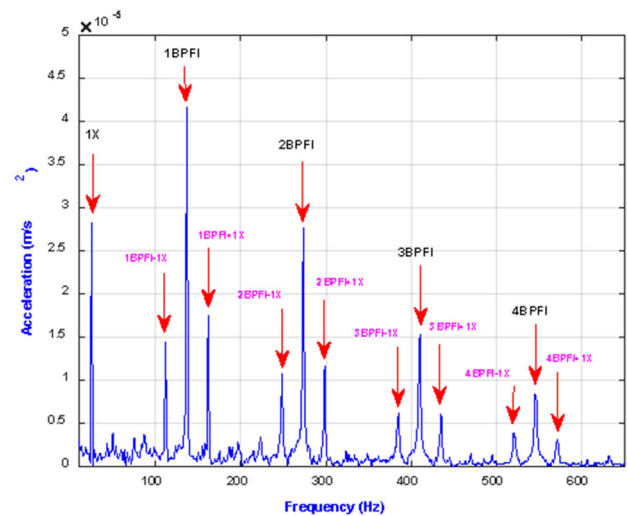
(d)

Fig. 4 Numerical results of the vibration response at the housing of defective bearing with defective inner ring at shaft speed of 1500 rpm (a) time record in horizontal direction, (b) envelope spectrum in horizontal direction, (c) time record in vertical direction and (d) envelope spectrum in vertical direction

(a)

(b)

(c)

(d)
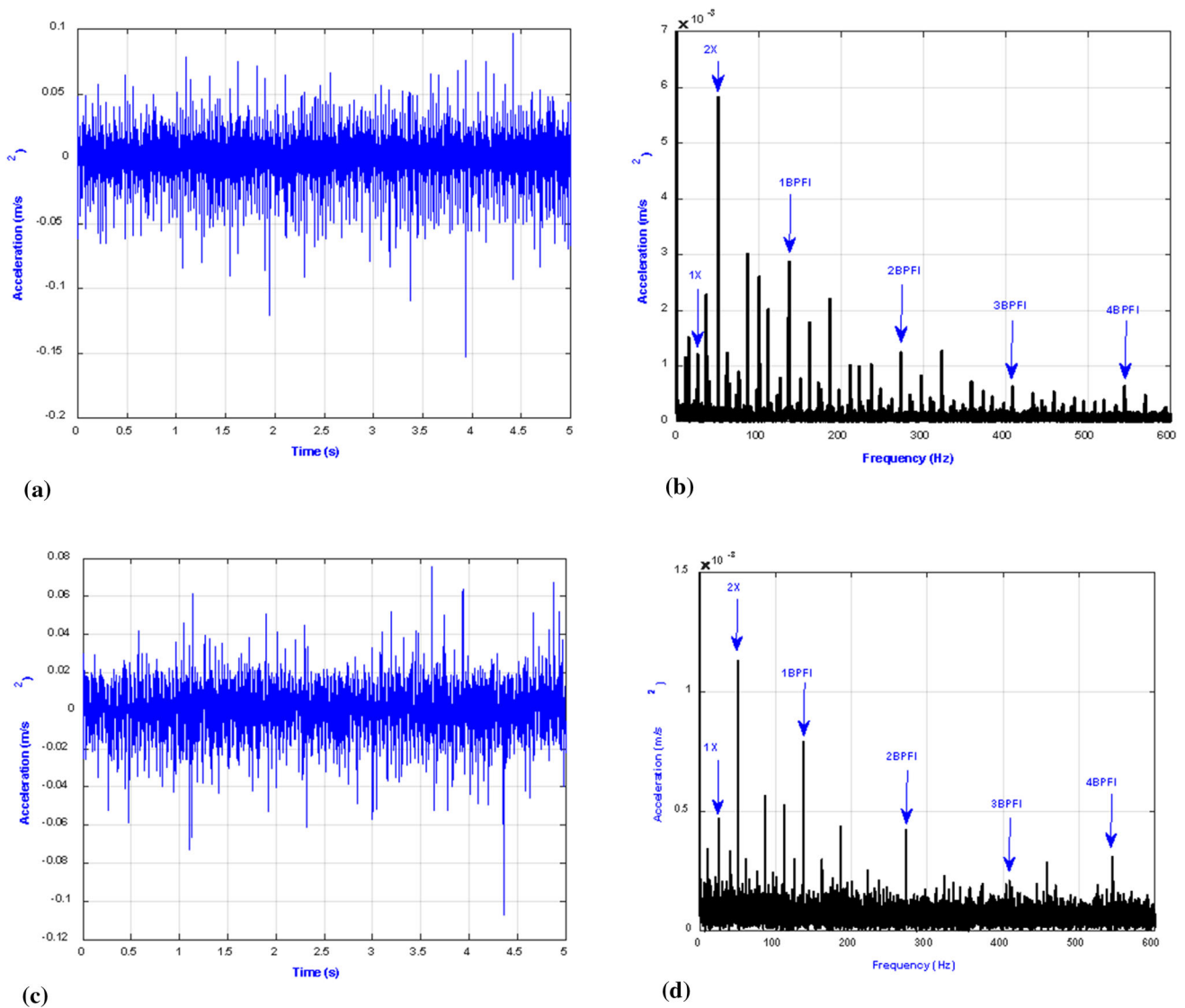
Fig. 5 Experimental vibration response at the housing of bearing with defective inner ring at shaft speed of 1500 rpm (**a**) time record in horizontal direction, (**b**) envelope spectrum in horizontal direction, (**c**) time record in vertical direction and (**d**) envelope spectrum in vertical direction

$$\omega_c = \left(1 - \frac{d}{D}\right)\frac{\omega_s}{2} \qquad \text{(Eq 12)}$$

where d is the rolling element diameter and D is the pitch diameter.

Simulation of Localized Defects

Defects on rings are shown schematically in Fig. 2.

Inner Ring faults

When the fault occurs in the inner ring, it is observed that the fault location on the inner ring doesn't stay stationary, because the inner ring and the shaft rotate with each other

at the same speed ω_s. As a result, the angle of the inner ring fault α_{in} is described as $\{\omega_s t \pm (\text{ fault width } / d_i)\}$. The deflection δ_i of the ith ball changes depending on whether the rolling ball approaching the fault is in the loaded or unloaded zone. The fault width can be used to describe the additional deflection Δ_j of the ball as it passes through the fault as follows [43]:

$$\Delta_j = \left(\frac{d}{2} - 0.5 * d * \cos(0.5 * \Phi_{ball})\right) \qquad \text{(Eq 13)}$$

where Φ_{ball} is the fault width of jth fault divided by radius of the ball. Hence, the location of the ith ball in the fault loaded zone can be described as [43]:

(a)

(b)

(c)

(d)
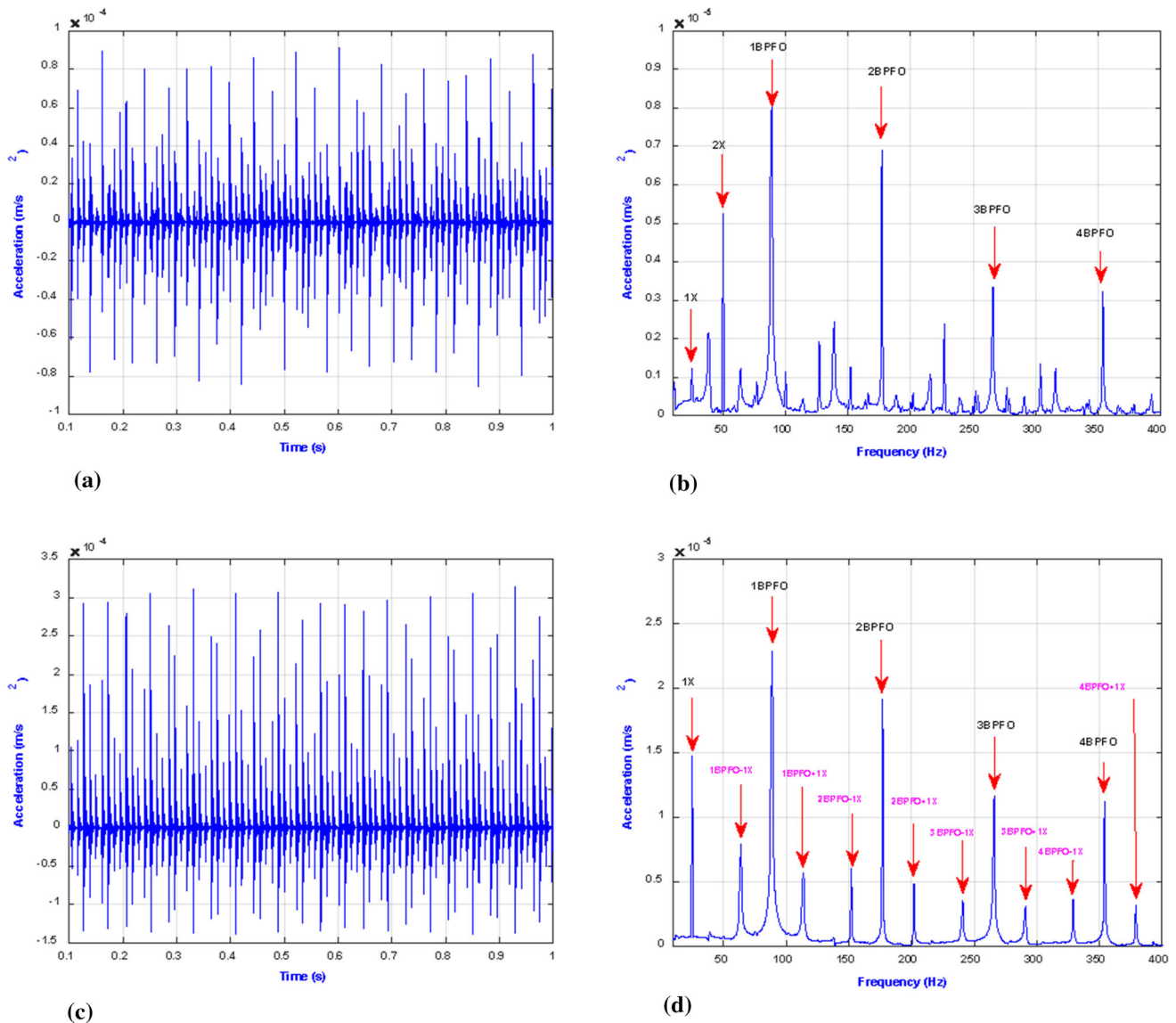
Fig. 6 Numerical results of the vibration response at the housing of bearing with defective outer ring at shaft speed of 1500 rpm (a) time record in horizontal direction, (b) envelope spectrum in horizontal direction, (c) time record in vertical direction and (d) envelope spectrum in vertical direction

$$\left(\omega_s t - \frac{\text{fault width}}{d_{in}}\right) \leq \varphi_i \leq \left(\omega_s t + \frac{\text{fault width}}{d_{in}}\right)$$

(Eq 14)

Outer Ring Fault

In contrast to the inner ring fault, the location fault in the case of the outer ring defect is typically seen in the bearing loaded zone. Furthermore, when the shaft rotates, the location of the fault remains stationary and does not vary. When the *i*th ball reaches the faulty zone of the outer ring,

its deflection varies. Thus, Eq. 15 can be used to describe the location of the *i*th ball in the fault loaded zone [43]:

$$\left(\alpha_{out} - \frac{\text{fault width}}{d_{out}}\right) \leq \varphi_i \leq \left(\alpha_{out} + \frac{\text{fault width}}{d_{out}}\right)$$

(Eq 15)

Experimental Setup

For validating the proposed mathematical model, measured signals for defective bearings are used. The measured vibration signals were adopted from [44] in which various defects were artificially created on a machinery fault

(a)

(b)

(c)

(d)
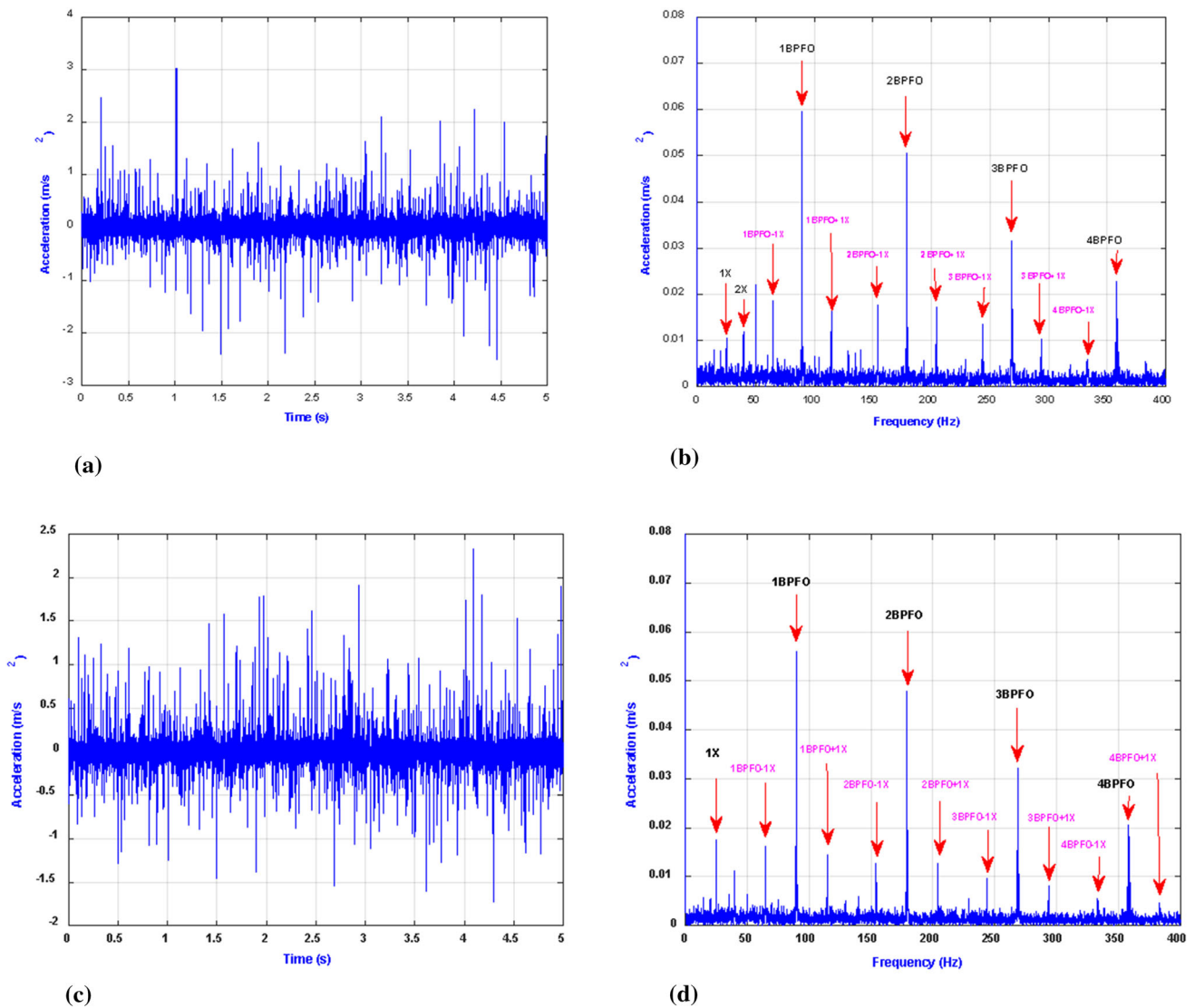
Fig. 7 Experimental response at the housing of defective bearing with defective outer ring at shaft speed of 1500 rpm (**a**) time record in horizontal direction, (**b**) Envelope spectrum in horizontal direction, (**c**) time record in vertical direction and (**d**) envelope spectrum in vertical direction

Table 3 Comparison of BPFI and BPFI obtained from the simulated model, using experiments and theoretical values

Speed	2000 rpm			2500 rpm		
	Model	Experimental	Theoretical	Model	Experimental	Theoretical
1X	33.4 Hz	33.5 Hz	33.33 Hz	41.67 Hz	41.8 Hz	41.66 Hz
BPFI	182 Hz	181.9 Hz	181.9 Hz	228 Hz	227.2 Hz	227.41 Hz
BPFO	118.3 Hz	119.8 Hz	118.06 Hz	147.8 Hz	149.8 Hz	147.6 Hz

demonstrator (PT 500) produced by G.U.N.T. located at the Faculty of Engineering-Mataria. The fault demonstrator as illustrated in Fig. 3 includes a steel shaft that carries one disk at its mid-span fastened using a taper lock. The shaft is supported by two deep groove ball bearings (SKF 6004) and coupled to an electric motor (0.37 kW) through a jaw coupling. Table 1 gives the physical details of the PT 500 rotor. The signals were sampled at a rate of 4000 Hz, for a total of 40,000 samples. Accelerometers were used to measure vibration signals in both horizontal and vertical directions.

1762

J Fail. Anal. and Preven. (2022) 22:1753–1770

Experimental Verification

In this section, the numerical and experimental results of a bearing having localized faults on the surfaces of the inner and outer rings are compared and analyzed. The rolling element bearing TYPE 6004 is used for the current study. The dimensions of the bearing can be approximately calculated by the expressions in [45]. The mass of the shaft, housing and sensor is found by weighing these elements using a precision scale. The stiffness and damping of the shaft are calculated by using free-free experimental measurements performed on the shaft. The values of the mass and stiffness of the unit resonator are selected such that

typical high-frequency resonant response of the bearing is simulated [46]. Table 2 shows the bearing characteristics as well as the fault parameters.

Defect on Inner Ring

Figure 4 shows the numerically computed vibration response of the bearing housing with a localized fault on the inner ring at a shaft rotational speed of 1500 rpm. The time domain in the horizontal and vertical directions is shown in Fig. 4a and c, respectively. The impulses created during the interaction of the balls and the faults are hard to
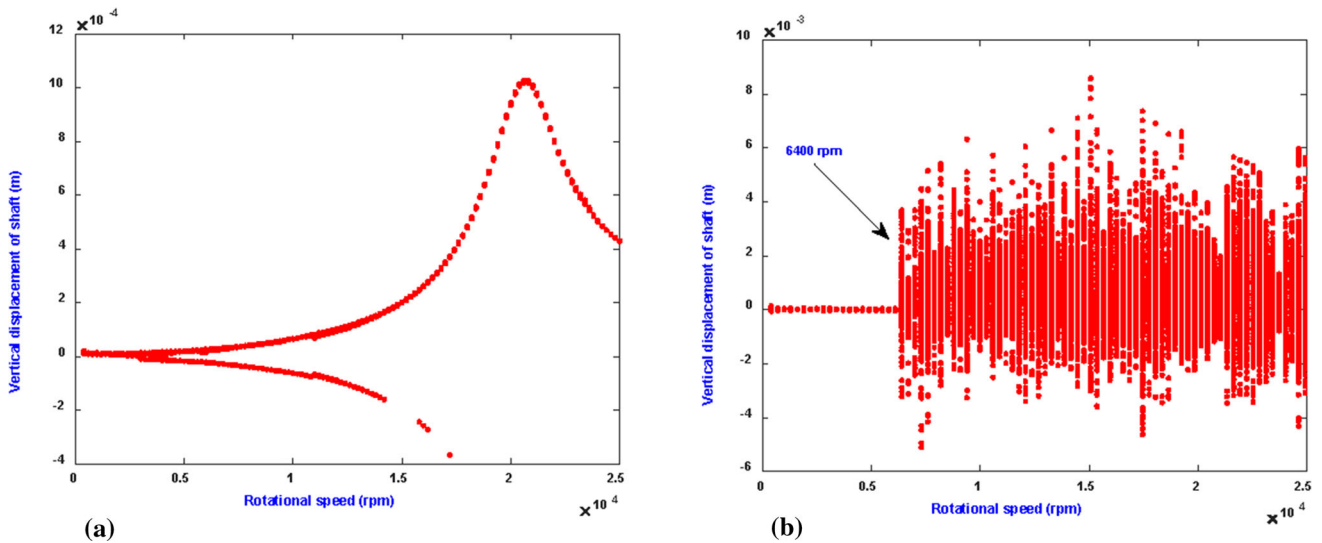
Fig. 8 Bifurcation diagram of the vertical displacement as a function of shaft speed (a) at width defect of 0.5 mm and (b) at width defect of 2 mm
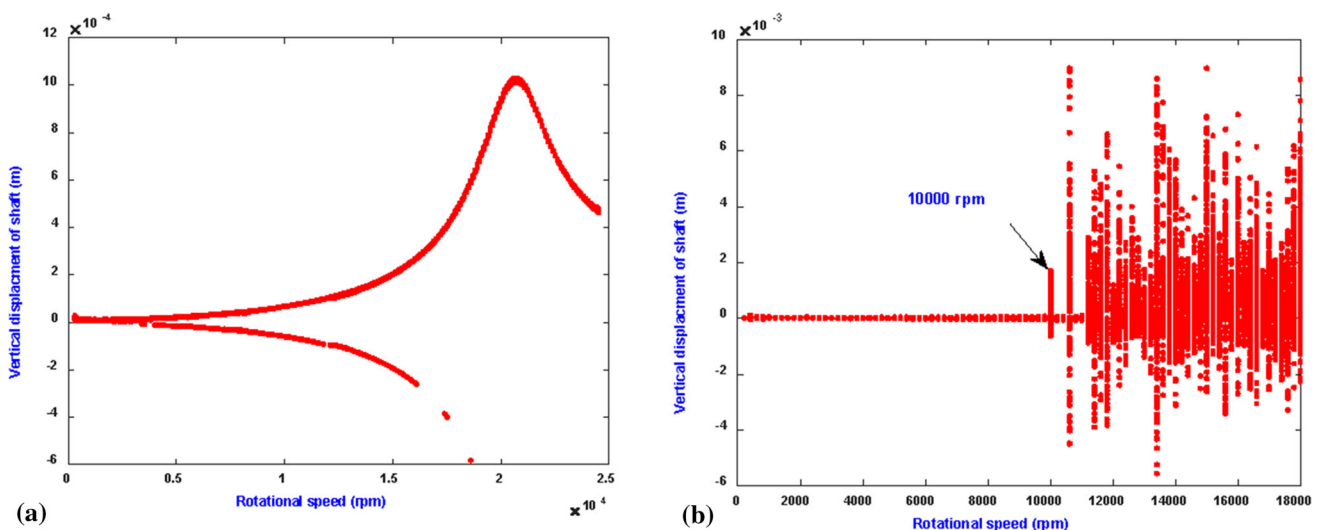
Fig. 9 Bifurcation diagram of the vertical displacement as a function of shaft speed (a) at width defect of 0.5 mm and (b) at width defect of 2 mm
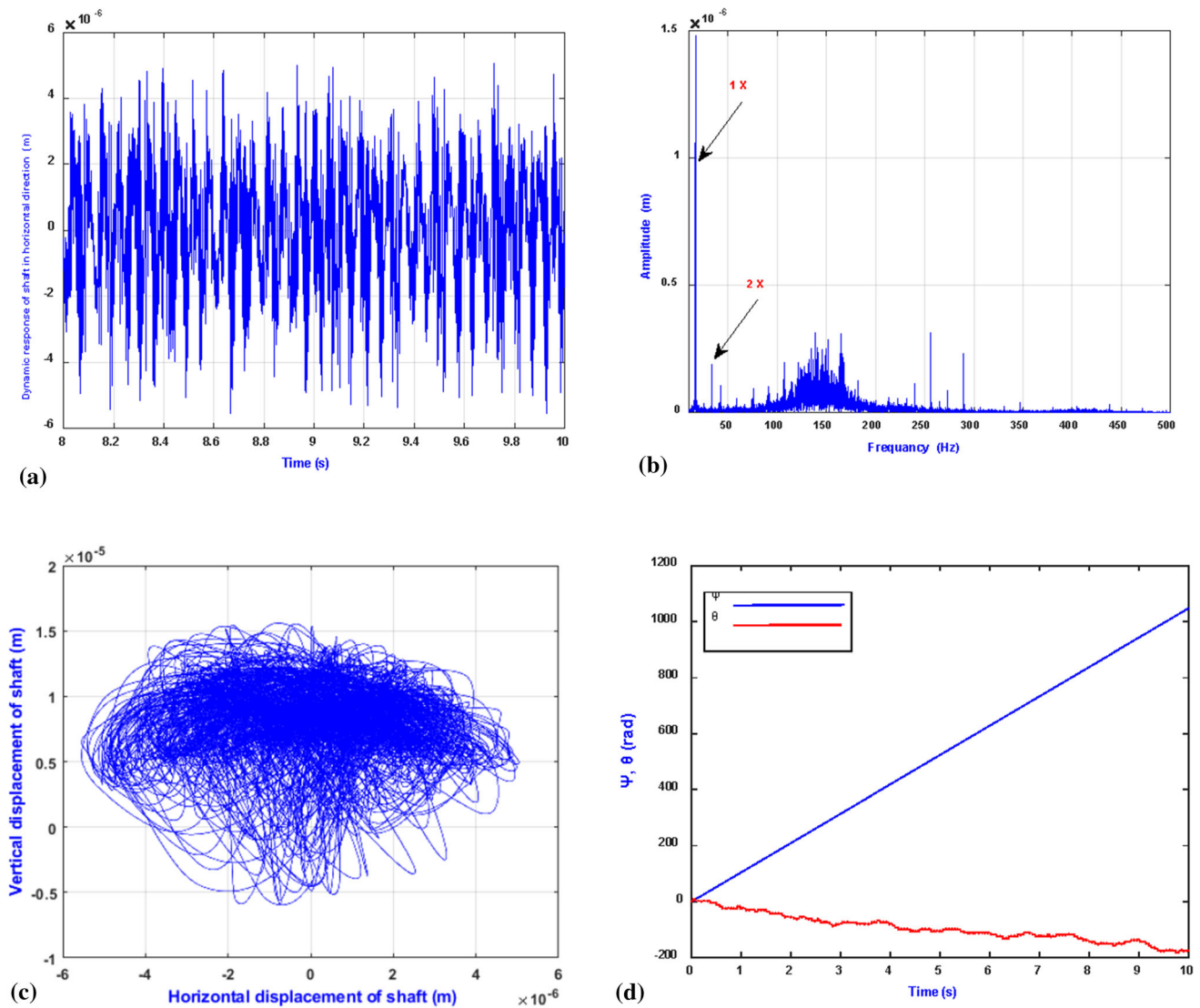
Fig. 10 Dynamic horizontal response of the bearing with inner ring fault at 1000 rpm (**a**) time waveform, (**b**) frequency spectrum, (**c**) orbit plot and (**d**) angular displacement showing backward whirling

distinguish in time domain because they are immersed in the noise caused by the dynamic load. As a result, for meaningful analysis, the vibration signal is better analyzed in the frequency domain. The theoretical characteristic defect frequency for a rotational speed equal to 1500 rpm (25 Hz) (the ball pass frequency for inner ring $(BPFI) = \frac{Nb}{2} * (Ns/60) * (1 + \frac{d}{D}))$ is computed as 136.45 Hz.

The envelope spectra based on the Hilbert transform of the signal in the horizontal and vertical directions at the shaft rotational speed of 1500 rpm are shown in Fig. 4b and d, respectively. The inner ring fault indicators in the envelope spectra can be clearly seen. The peaks at the shaft rotational frequency (1X), BPFI and a series of harmonics of BPFI with sidebands spaced at shaft speed around BPFI and its harmonics, as well as harmonics of the shaft speed,

are shown in Fig. 4b and d. At shaft rotational speed 1500 rpm, the BPFI peak is identified at 136 Hz, which is close to the predicted value of BPFI (136.45 Hz).

To more effectively determine the validity of the simulation model of faulty inner ring rolling element bearings, experimental data from a defective 6004 bearing with a fault in its inner ring are employed. Figure 5a and c illustrates the experimental vibration spectrum at the housing of the bearing with inner ring defect at the shaft's rotational speed of 1500 rpm in both horizontal and vertical directions, respectively. Figure 5b and d shows the envelope spectrum at the housing of the bearing at the shaft's rotational speed of 1500 rpm in both horizontal and vertical directions, respectively. Figure 5b and d shows a series of harmonics of BPFI. In the vertical envelope spectrum, side bands are masked by the background noise.

1764

J Fail. Anal. and Preven. (2022) 22:1753–1770
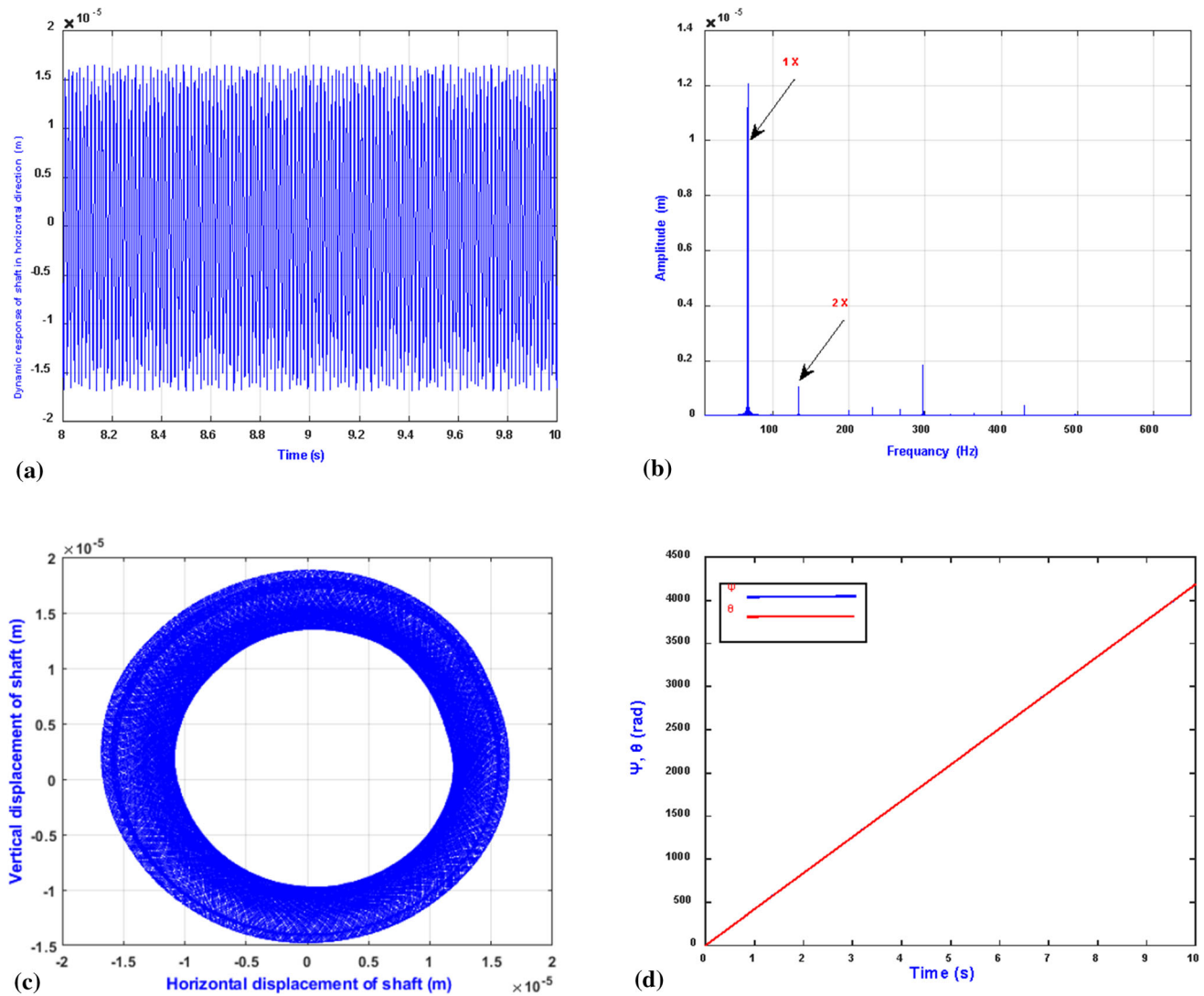
Fig. 11 Dynamic horizontal response of the bearing with inner ring fault at 4000 rpm (**a**) time waveform, (**b**) frequency spectrum, (**c**) orbit plot and (**d**) angular displacement showing forward whirling

The BPFI peaks are found at 136.1 Hz, which is very close to the theoretical value of BPFI (136.45 Hz) and the calculated value from the proposed model (136 Hz). This small variation in frequency may be attributed to a small variation in shaft speed.

Defect on Outer Ring

Figure 6 shows the computed results of the vibration time responses and envelope spectra at the housing of the bearing having localized defect on the surface of the outer ring in both horizontal and vertical directions, respectively, at the shaft rotational speed of 1500 rpm. Figure 6b and d shows the envelope spectrum at the housing of the bearing at the shaft's rotational speed of 1500 rpm in both horizontal and vertical directions, respectively. Figure 6b and d

shows the peaks at shaft rotation frequency (1X), harmonics of 1X, BPFO and a series of harmonics of BPFO. Sidebands spaced at shaft speed can be obviously seen around each harmonic in the vertical envelope spectra. The BPFO peak is found at 89 Hz at the shaft rotational speed of 1500 rpm which is close to the theoretical value of BPFO (89.5 Hz).

Figure 7 demonstrates the experimental vibration spectrum at the housing of the bearing with outer ring defect in the bearing at the shaft rotational speed of 1500 rpm in horizontal and vertical directions, respectively. Similar results to the numerical results can be seen; however, the side bands are obvious in both horizontal and vertical envelope spectra as shown in Figs. 7b and d. The BPFO peak is detected at 89.6 Hz, which is close to the theoretical BPFO value (89.5 Hz) and the calculated value from proposed model (89 Hz).
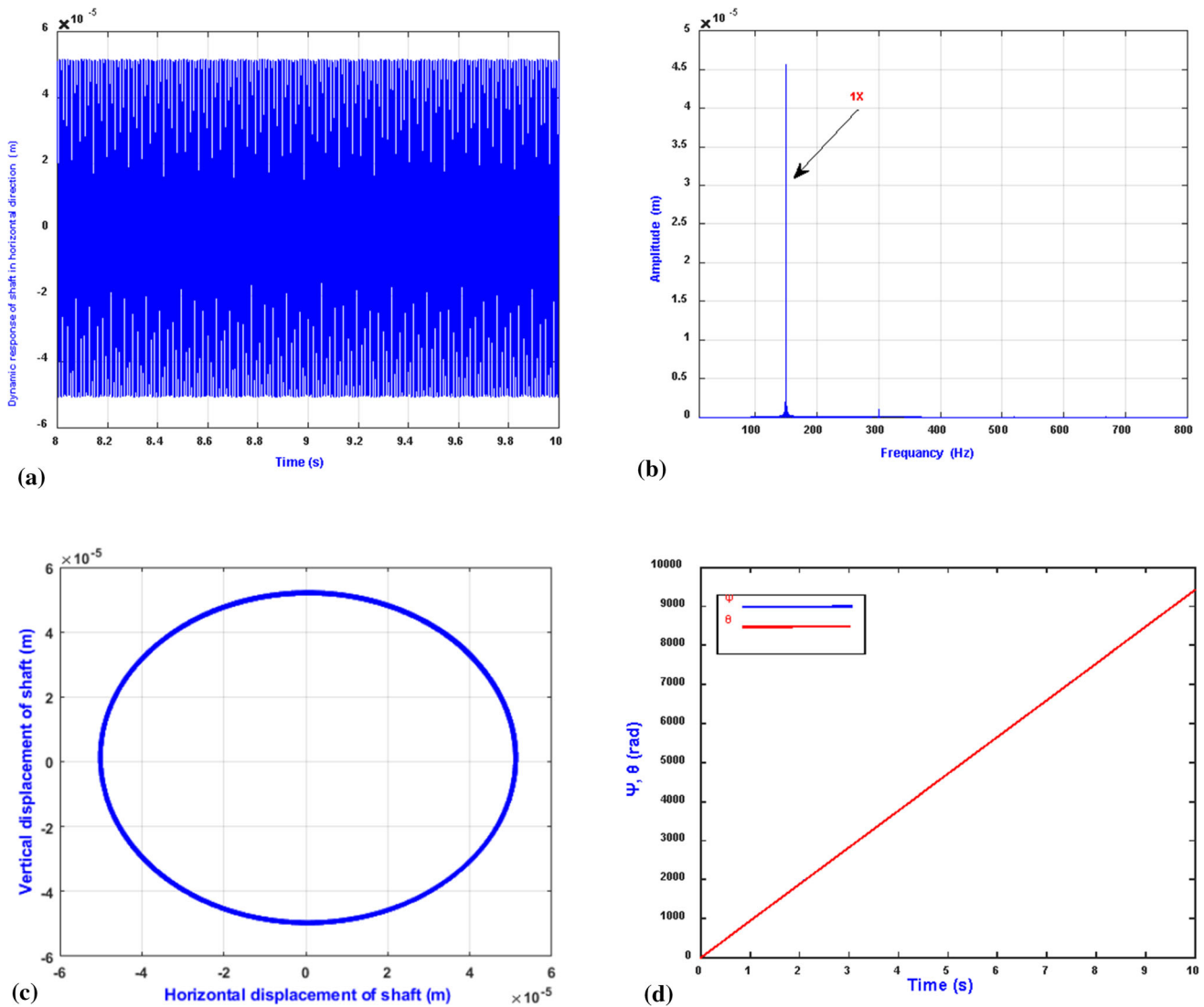
Fig. 12 Dynamic horizontal response of the bearing with inner ring fault at 9000 rpm (**a**) time waveform, (**b**) frequency spectrum, (**c**) orbit plot and (**d**) angular displacement showing forward whirling

Comparison between Experimental Results and Numerical Results

A comparison between experimental results and numerical results for inner ring fault and outer ring fault at different speeds is summarized in Table 3. The results show very good agreement between numerical and experimental analysis. Hence, the proposed model is shown to yield accurate results when compared with experimental results.

Parametric study

The Effect of the Fault Width

Figure 8 shows the effect of the defect width on the rotor response, where the bearing is having a localized defect on

the surface of the inner ring at two different values of defect width: 0.5 and 2 mm at different shaft rotational speeds. The results are displayed as a bifurcation diagram of the vertical displacement of the shaft. Figure 8a shows the vertical displacement at defect width 0.5 mm. The response amplitude is shown to increase gradually with the increase in shaft speed until reaching the maximum at the critical speed (20,600 rpm) and then decreases gradually. Figure 8b shows the vertical displacement at defect width 2 mm, with the increase in the width of the defect, and it was found that the response shows chaotic motion when the shaft speed increases to higher than 6400 rpm.

Figure 9 illustrates the influence of fault width on rotor behavior in a bearing with a localized fault on the outer ring surface at two different defect widths of 0.5 and 2 mm at two different shaft rotational speeds. The results are shown as a bifurcation diagram of the vertical displacement

1766

J Fail. Anal. and Preven. (2022) 22:1753–1770
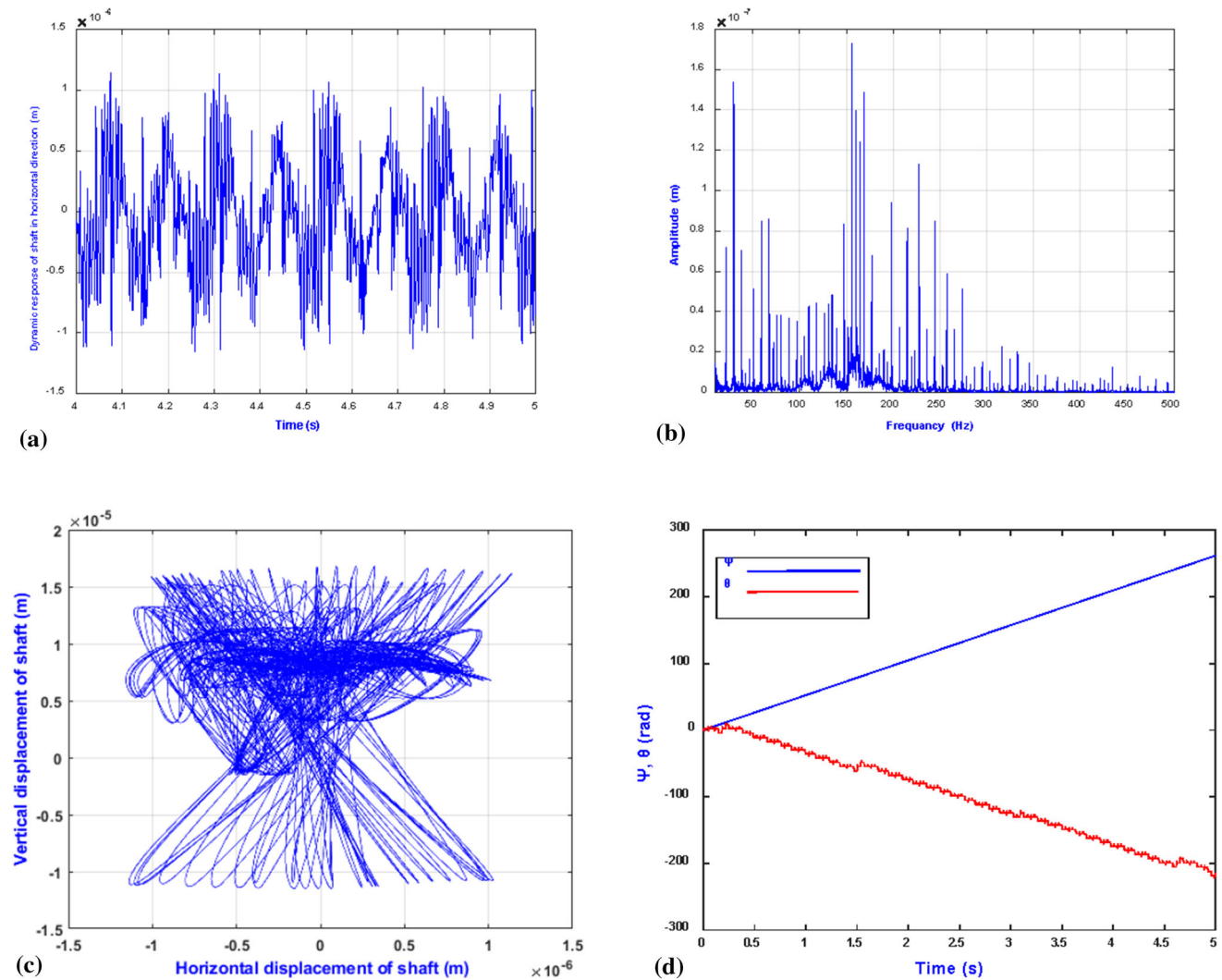
Fig. 13 Dynamic horizontal response of the bearing with outer ring fault at 500 rpm (**a**) time waveform, (**b**) frequency spectrum, (**c**) orbit plot and (**d**) angular displacement showing backward whirling

of shaft versus the rotational speed. Figure 9a shows the vertical displacement at a defect width of 0.5 mm. The response amplitude increases with shaft speed until it reaches its maximum at the critical speed (20,600 rpm), after which it gradually decreases. Figure 9b shows the vertical displacement at defect width 2 mm. With the increase in the width of the defect, it was found that the response becomes chaotic above shaft speed of 10,000 rpm.

Effect of Rotational Shaft Speed

Figure 10 shows the frequency spectrum in horizontal direction and the orbit plots for the shaft center at different rotational shaft speeds. The bearing has a localized defect on the surface of the inner ring. At 1000 rpm, noise in the

frequency spectrum in Fig. 10b is a strong indication of the chaotic nature of the response. Figure 10c and d shows a chaotic orbit with backward whirling.

With increasing speed, the noise intensity decreased, and the system vibration behavior becomes quasi-periodic. Figure 11b shows the frequency spectrum at 4000 rpm. Figure 11c and d shows a quasi-periodic orbit with forward whirling.

As speed is increased, the orbit shape changes to form a semi-elliptical shape at higher speed (at 9000 rpm), because the increased unbalance force causes the 1X component to dominate over the varying compliance and subharmonic frequencies. Hence, the system vibration behavior transforms to periodic motion with forward whirling as shown in Fig. 12c and d.

Figure 13 shows the horizontal frequency spectrum and orbit plots for the shaft center at various rotational speeds

J Fail. Anal. and Preven. (2022) 22:1753–1770

1767
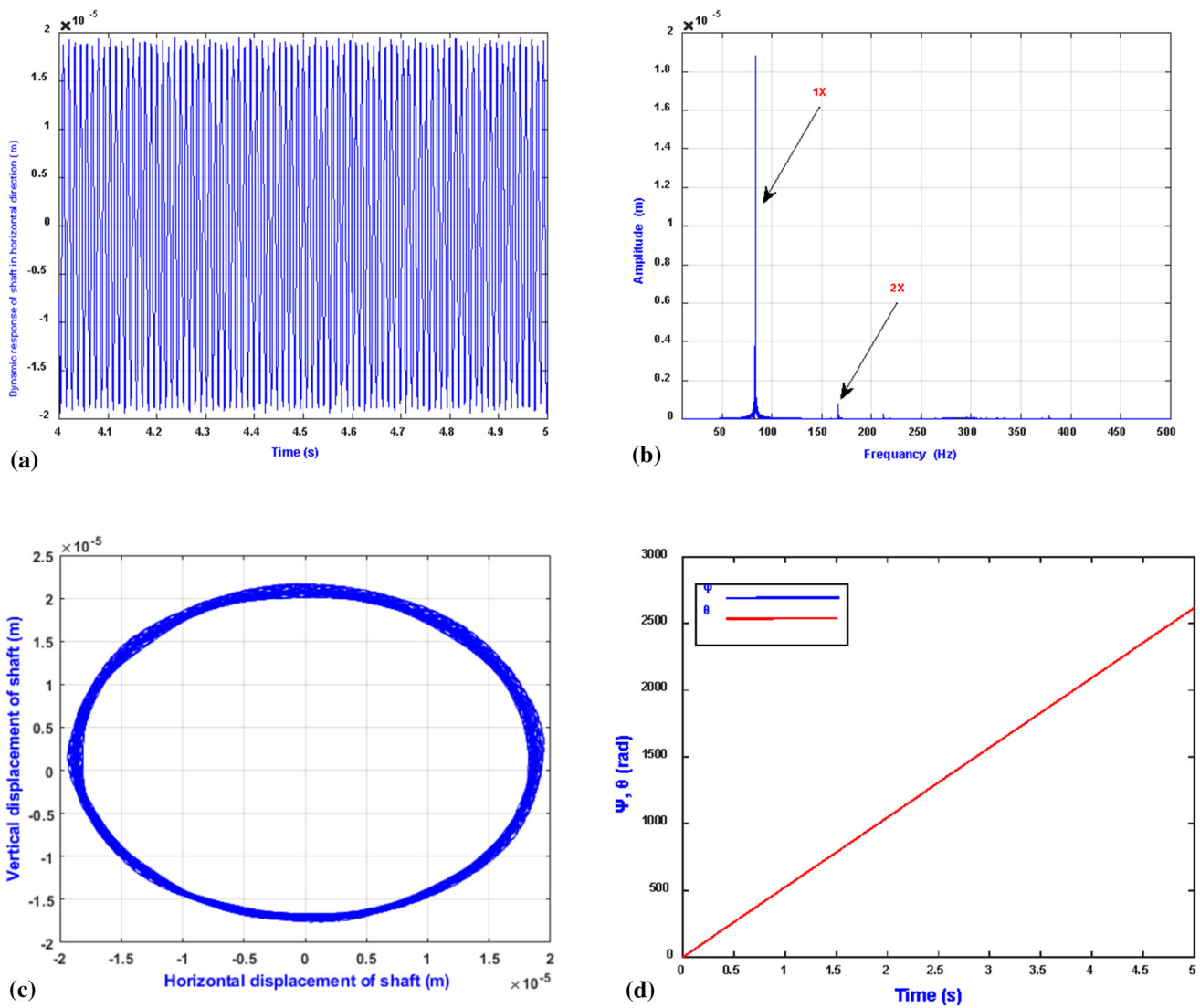
Fig. 14 Dynamic horizontal response of the bearing with outer ring fault at 5000 rpm (**a**) time waveform, (**b**) frequency spectrum, (**c**) orbit plot and (**d**) angular displacement showing forward whirling

for the case of outer ring fault. Noise in the frequency spectrum at 500 rpm (Fig. 13b) is clear evidence of the chaotic nature of the system, and a chaotic orbit with backward whirling is shown in Fig. 13c and d.

As the speed increases (at 5000 rpm), the noise level is reduced (Fig. 14b), and the system vibration behavior becomes quasi-periodic. Figure 14c shows a quasi-periodic orbit with forward whirling at this speed.

At 10,000 rpm, periodic forward orbit is shown in Fig. 15c and d.

Conclusions

The nonlinear dynamic response of a rolling element bearing with localized defects on the inner ring and outer ring is investigated. First, the numerical model is validated against experimental results. The envelope spectra of the simulated signals are shown to have the characteristic vibration patterns of bearing faults as the envelope spectra of the measured signals. Furthermore, a parametric study is presented to show the effect of varying the rotational speed and the defect size on the bearing response. Both the nature of response and the direction of whirling are studied. Based on the presented results, the following conclusions may be drawn:

The rotational speed is shown to have a crucial effect on the bearing response. At lower speeds, the response is mainly chaotic with backward whirling. Increasing speed will cause forward whirling and the response changes to quasi-periodic and then reaches periodic motion at higher speeds. This is observed for both inner ring and outer ring faults. However, the defect width increase is shown to cause dominant chaotic motion even at high speeds. The
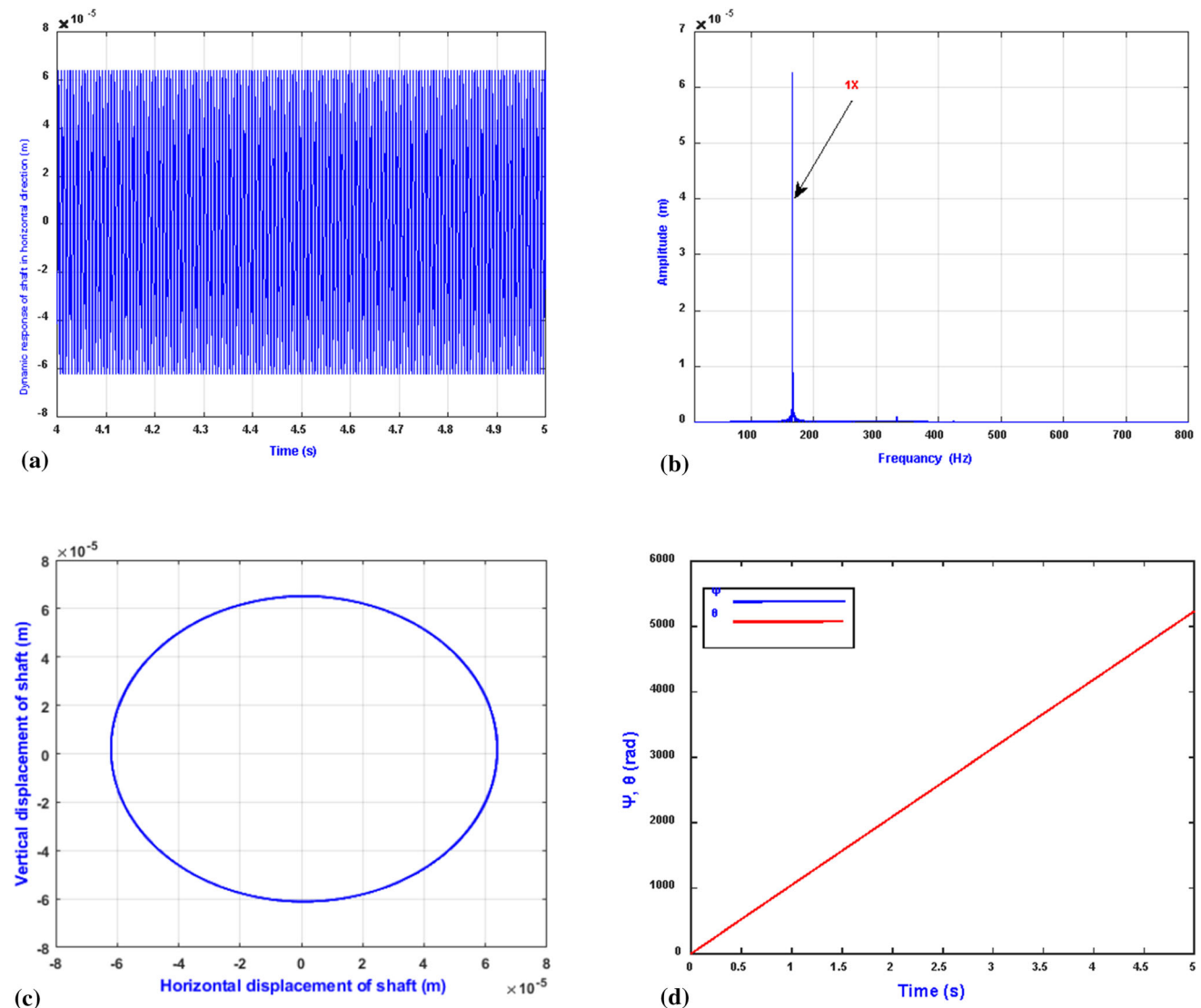
Fig. 15 Dynamic horizontal response of the bearing with outer ring fault at 10,000 rpm (**a**) time waveform, (**b**) frequency spectrum, (**c**) orbit plot and (**d**) angular displacement showing forward whirling

onset of chaos is observed to occur for the inner ring fault at lower speed in comparison with the outer ring fault. For the bearing considered in this study, the impulses due to defects were clearly noticed in the time waveform at lower speeds for the early stage of the defects. The good agreement between the simulated numerical results and the measured results suggests that the presented model can efficiently predict the nonlinear response of bearing with localized defects.

References

1. G.K. Singh, S.A. Ahmed Saleh Al Kazzaz, Induction machine drive condition monitoring and diagnostic research—a survey. Electr. Power Sys. Res. **64**(2), 145–158 (2003)
2. N. Tandon, A. Choudhury, A review of vibration and acoustic measurement methods for the detection of defects in rolling element bearings. Tribol. Int. **32**(8), 469–480 (1999)
3. A. Sharma et al., Nonlinear dynamic investigations on rolling element bearings: a review. Adv. Mech. Eng. **10**(3), 1687814018764148 (2018)

4. Patil, M.S., J. Mathew, and P.K. RajendraKumar, *Bearing Signature Analysis as a Medium for Fault Detection: A Review.* Journal of Tribology, 2007. **130**(1).

5. H.D.M. de Azevedo, A.M. Araújo, N. Bouchonneau, A review of wind turbine bearing condition monitoring: state of the art and challenges. Renew. Sustain. Energy Rev. **56**, 368–379 (2016)

6. S. Singh, C.Q. Howard, C.H. Hansen, An extensive review of vibration modelling of rolling element bearings with localised and extended defects. J. Sound Vib. **357**, 300–330 (2015)

7. H. Cheng et al., Research on ball bearing model based on local defects. SN Appl. Sci. **1**(10), 1–10 (2019)

8. S.S. Kulkarni, A.K. Bewoor, R.B. Ingle, Vibration signature analysis of distributed defects in ball bearing using wavelet decomposition technique. Noise & Vib. Worldw. **48**(1–2), 7–18 (2017)

9. S. Kulkarni, S.B. Wadkar, Experimental investigation for distributed defects in ball bearing using vibration signature analysis. Proc. Eng. **144**, 781–789 (2016)

10. V.K. Rai, A.R. Mohanty, Bearing fault diagnosis using FFT of intrinsic mode functions in Hilbert-Huang transform. Mech. Syst. Signal Process. **21**(6), 2607–2615 (2007)

11. W. Sun et al., Fault diagnosis of rolling bearing based on wavelet transform and envelope spectrum correlation. J. Vib. Control. **19**(6), 924–941 (2013)

12. J. Chen et al., Generator bearing fault diagnosis for wind turbine via empirical wavelet transform using measured vibration signals. Renew. Energy. **89**, 80–92 (2016)

13. H.H. El-Mongy, *Feature extraction enhancement based on parameterless empirical wavelet transform: Application to bearing fault diagnosis.* in *18th International Conference on Applied Mechanics and Mechanical Engineering (AMME).* Military Technical College, Cairo, Egypt, 2018.

14. K. Zhang et al., Feature extraction method based on adaptive and concise empirical wavelet transform and its applications in bearing fault diagnosis. Measurement. **172**, 108976 (2021)

15. J. Zheng et al., Adaptive power spectrum Fourier decomposition method with application in fault diagnosis for rolling bearing. Measurement. **183**, 109837 (2021)

16. Kong, F. et al., A vibration model of ball bearings with a localized defect based on the hertzian contact stress distribution. Shock and Vibration, (2018)

17. P.D. McFadden, J.D. Smith, Model for the vibration produced by a single point defect in a rolling element bearing. J. Sound Vib. **96**(1), 69–82 (1984)

18. P.D. McFadden, J.D. Smith, The vibration produced by multiple point defects in a rolling element bearing. J. Sound Vib. **98**(2), 263–273 (1985)

19. N. Tandon, A. Choudhury, An analytical model for the prediction of the vibration response of rolling element bearings due to a localized defect. J. Sound Vib. **205**(3), 275–292 (1997)

20. M.S. Patil et al., A theoretical model to predict the effect of localized defect on vibrations associated with ball bearing. Int. J. Mech. Sci. **52**(9), 1193–1201 (2010)

21. B. Changqing, X. Qingyu, Dynamic model of ball bearings with internal clearance and waviness. J. Sound Vib. **294**(1), 23–48 (2006)

22. Zhang, X. et al., Dynamic modeling and analysis of rolling bearing with compound fault on raceway and rolling element. Shock and Vibration, 2020.

23. W. Liqin et al., Nonlinear dynamics behaviors of a rotor roller bearing system with radial clearances and waviness considered. Chin. J. Aeronaut. **21**(1), 86–96 (2008)

24. Arslan, H. Aktürk, N. An Investigation of Rolling Element Vibrations Caused by Local Defects. Journal of Tribology, **130**(4). (2008)

25. Kankar, P.K., S.C. Sharma, and S.P. Harsha, Fault Diagnosis of High Speed Rolling Element Bearings Due to Localized Defects Using Response Surface Method. Journal of Dynamic Systems, Measurement, and Control, 2011. **133**(3).

26. A. Rafsanjani et al., Nonlinear dynamic modeling of surface defects in rolling element bearing systems. J. Sound Vib. **319**(3), 1150–1174 (2009)

27. M. Tiwari, K. Gupta, O. Prakash, Effect of radial internal clearance of a ball bearing on the dynamics of a balanced horizontal rotor. J. Sound Vib. **238**(5), 723–756 (2000)

28. S.P. Harsha, Nonlinear dynamic analysis of an unbalanced rotor supported by roller bearing. Chaos, Solitons Fractals. **26**(1), 47–66 (2005)

29. S.H. Ghafari, F. Golnaraghi, F. Ismail, Effect of localized faults on chaotic vibration of rolling element bearings. Nonlinear Dyn. **53**(4), 287–301 (2008)

30. Gupta, T.C., K. Gupta, and D.K. Sehgal, Instability and chaos of a flexible rotor ball bearing system: an investigation on the influence of rotating imbalance and bearing clearance. Journal of engineering for gas turbines and powe. **133**(8). (2011)

31. M. Tadina, M. Boltežar, Improved model of a ball bearing for the simulation of vibration signals due to faults during run-up. J. Sound Vib. **330**(17), 4287–4301 (2011)

32. F. Cong et al., Vibration model of rolling element bearings in a rotor-bearing system for fault diagnosis. J. Sound Vib. **332**(8), 2081–2097 (2013)

33. D.H. Pandya, S.H. Upadhyay, S.P. Harsha, Nonlinear dynamic analysis of high speed bearings due to combined localized defects. J. Vib. Control. **20**(15), 2300–2313 (2014)

34. L. Cui, X. Chen, S. Chen, Dynamics modeling and analysis of local fault of rolling element bearing. Adv. Mech. Eng. **7**(1), 262351 (2015)

35. L. Cui et al., Vibration response mechanism of faulty outer race rolling element bearings for quantitative analysis. J. Sound Vib. **364**, 67–76 (2016)

36. C. Mishra, A.K. Samantaray, G. Chakraborty, Ball bearing defect models: a study of simulated and experimental fault signatures. J. Sound Vib. **400**, 86–112 (2017)

37. K. Kappaganthu, C. Nataraj, Nonlinear modeling and analysis of a rolling element bearing with a clearance. Commun. Nonlinear Sci. Numer. Simul. **16**(10), 4134–4145 (2011)

38. I. Rehab et al., The influence of rolling bearing clearances on diagnostic signatures based on a numerical simulation and experimental evaluation. Int. J. Hydromechatronics. **1**(1), 16–46 (2018)

39. H. Wang, Q. Han, D. Zhou, Nonlinear dynamic modeling of rotor system supported by angular contact ball bearings. Mech. Syst. Signal Process. **85**, 16–40 (2017)

40. F. Kong et al., Research on effect of damping variation on vibration response of defective bearings. Adv. Mech. Eng. **11**(3), 1687814019827733 (2019)

41. J. Wang et al., Online bearing clearance monitoring based on an accurate vibration analysis. Energies. **13**(2), 389 (2020)

42. M. Liang et al., Effect of rolling bearing parameters on the nonlinear dynamics of offset rotor. Proc. Inst. Mech. Eng. C J. Mech. Eng. Sci. **234**(15), 2968–2978 (2020)

43. V.N. Patel, N. Tandon, R.K. Pandey, A dynamic model for vibration studies of deep groove ball bearings considering single and multiple defects in races. ASME. J. Tribol. **132**(4), 041101 (2010)

44. H.H. El-Mongy, O. Abdel-Naby, H. Abdel-Nour, M.A. Elkady, H.M. Fathy, M.T. Hassan, N.G. Heikal, H.A. Mohamed, M.H. Mohamed, A.M. Reda, A.T. Sultan, *A theoretical and experimental study on fault diagnosis of rotating machines using vibration analysis.* Graduation project technical report, Helwan University, Cairo, Egypt, 2019.

1770

J Fail. Anal. and Preven. (2022) 22:1753–1770

45. Tiwari, R., *Rotor systems: analysis and identification*. 2017: CRC press.

46. N. Sawalhi, R.B. Randall, Simulating gear and bearing interactions in the presence of faults: Part I. The combined gear bearing dynamic model and the simulation of localised bearing faults. Mech. Sys. Sig. Process. **22**(8), 1924–1951 (2008)